FULL PAPER

ADVANCED
FUNCTIONAL
MATERIALS

www.afm-journal.d

Check for
updates

Enhanced Sensitivity of Iontronic Graphene Tactile Sensors Facilitated by Spreading of Ionic Liquid Pinned on Graphene Grid

Joo Sung Kim, Seung Chul Lee, Jinhyun Hwang, Eunho Lee, Kilwon Cho, Sung-Jin Kim, Do Hwan Kim,* and Wi Hyoung Lee*

Iontronic graphene tactile sensors (i-GTS) composed of a top floating graphene electrode and an ionic liquid droplet pinned on a bottom graphene grid, which can dramatically enhance the performance of capacitive-type tactile sensors, are presented. When mechanical stress is applied to the top floating electrode, the i-GTS operates in one of the following three regimes: air–air, air–electric double layer (EDL) transition, or EDL–EDL. Once the top electrode contacts the ionic liquid in the i-GTS, the spreading behavior of the ionic liquid causes a capacitance transition (from a few pF to over hundreds of pF). This is because EDLs are formed at the interfaces between the electrodes and the ionic liquid. In this case, the pressure sensitivity increases to ≈31.1 kPa⁻¹ with a gentle touch. Under prolonged application of pressure, the capacitance increases gradually, mainly due to the contact line expansion of the ionic liquid bridge pinned on the graphene grid. The sensors exhibit outstanding properties (response and relaxation times below 80 ms, and stability over 300 cycles) while demonstrating ultimate signal-to-noise ratios in the array tests. The contact-induced spreading behavior of the ionic liquid is the key for boosting the sensor performance.

1. Introduction

Tactile sensors based on nanocarbon materials (such as carbon nanotubes and graphene) have been widely investigated for use in the development of transparent and flexible electronic skins (e-skins).[1–5] Various types of the tactile sensors have been developed for the instantaneous detection of pressure.[6–8] Capacitive-type tactile sensors based on deformable organic materials have the advantages of excellent sensitivity and repeatability.[9–12] However, their low signal-to-noise ratio, inconsistent sensing capability over a wide range of pressures, and unstable operation caused by the viscoelastic properties of the elastomer are problematic for their commercialization.[6,13–15] In particular, their change in capacitance under gentle pressure is only in the range of a few pF, requiring highly sensitive inductance capacitance resistance (LCR) meters.[9,16–18] To overcome these drawbacks, ionic liquids with extremely high capacitance can be used as the active dielectric medium, and special cell designs for inducing changes in the contact area at the electrical double layer (EDL) have been demonstrated for the fabrication of high-gain pressure sensors.[19–23]

In this regard, the use of liquid droplets in tactile sensors can optimize both the mechanical properties and sensing characteristics. For instance, the liquid metal eutectic gallium-indium (EGaIn) has been proven useful in the fabrication of micro-droplet-based multifunctional e-skins.[24] Ionic liquid droplets confined in elastomers exhibit acute pressure-sensing properties with mechanical bendability.[20,21,25] However, all the previous studies that utilized ionic liquid droplets in tactile sensors used only ionic liquid droplets confined in closed cells, where the liquid droplet was in contact with the top and bottom electrodes.[19–23,25] Owing to the high initial capacitance caused by EDL formation at the interface between the ionic liquid and the electrode, these approaches were not effective for fabricating sensitive pressure sensors with high signal-to-noise ratios. We noticed that the use of a top floating electrode could improve the dynamic characteristics of liquid droplets, thereby boosting the sensitivity and signal-to-noise ratio of droplet-based tactile sensors.

J. S. Kim, Prof. D. H. Kim
Department of Chemical Engineering
Hanyang University
Seoul 04763, South Korea
E-mail: dhkim76@hanyang.ac.kr

S. C. Lee, J. Hwang, Prof. W. H. Lee
Department of Organic and Nano System Engineering
Konkuk University
Seoul 05029, South Korea
E-mail: whlee78@konkuk.ac.kr

Dr. E. Lee, Prof. K. Cho
Department of Chemical Engineering
Pohang University of Science and Technology (POSTECH)
Pohang 37673, South Korea

Prof. S.-J. Kim
Department of Mechanical Engineering
Konkuk University
Seoul 05029, South Korea

Prof. D. H. Kim
Institute of Nano Science and Technology
Hanyang University
Seoul 04763, South Korea

The ORCID identification number(s) for the author(s) of this article can be found under https://doi.org/10.1002/adfm.201908993.

DOI: 10.1002/adfm.201908993

In this work, we describe flexible iontronic graphene tactile sensors (i-GTS) with superior sensitivity, composed of top floating graphene electrodes and ionic liquid droplets pinned on bottom graphene grid electrodes. The transparency of the i-GTS is maximized by using chemical vapor deposition (CVD)-grown graphene as the top and bottom electrodes. The confinement of the ionic liquid droplet is accomplished by placing the ionic liquid droplet on the bottom graphene electrode, which is patterned with grid relief. The unique cell design in this work can induce dynamic characteristics in the liquid droplet when the top floating graphene electrode contacts the ionic liquid droplet, and generate spreading behavior under gentle touch. The tactile sensors achieve superior sensitivity at this transitional step. In particular, we can effectively control the transitional step that determines the pressure range by changing several elements of the i-GTS, such as the droplet size. Finally, an i-GTS array with extremely high signal-to-noise ratio is demonstrated.

2. Results and Discussion

Figure 1a shows a schematic of the fabrication process of the proposed i-GTS based on an ionic liquid pinned on a graphene grid. Detailed explanations on the experimental procedure can be found in the Experimental Section. Generally, the hydrophobicity of pristine graphene surfaces is not sufficient for inducing dewetting of the ionic liquid. Thus, in this study, the graphene surface was treated with octadecyltrichlorosilane (ODTS) to allow low surface energy, because surface defects in graphene could provide anchoring sites for the self-assembly of ODTS on the graphene surface.[26,27] The water contact angle was changed from 85° to 104.5° after the deposition of ODTS, proving that the ODTS treatment was effective in reducing the surface energy of graphene (see Figure S1 in the Supporting Information). Considering that the water contact angle of well-ordered ODTS monolayers on SiO_2/Si was reported to be greater than 105°, the ODTS layer on our graphene surface could contain disordered regions with structural defects.[27] Further, prolonged exposure of UV/O_3 on ODTS/graphene resulted in the etching of ODTS and graphene. This etching process is a critical step in the development of graphene grid films, which can potentially serve ultrasensitive i-GTS. When the exposure time is over 60 min, ODTS/graphene is fully etched, as shown in the Raman spectra of Figure S2 in the Supporting Information. The contact angle of water on UV/O_3-treated ODTS/graphene was measured to be less than 20°, which was sufficient for enabling wetting/dewetting-induced patterning of the ionic liquid (Figure S1 in the Supporting Information). The spin-casting of the ionic liquid, 1-ethyl-3-methylimidazolium tetrafluoroborate ($[EMIM]^+[BF_4]^-$) resulted in its preferential formation at the contact line of the graphene grid (see Figure S3 and Movie S1 in the Supporting Information). 1-Ethyl-3-methylimidazolium tetrafluoroborate was chosen because it exhibits both high ionic conductivity and low viscosity. The top floating graphene electrode on the polyethylene terephthalate (PET) substrate was placed on a photoresist spacer to fabricate the metal–insulator–metal (MIM) capacitor.

The operating principle of the i-GTS with top floating graphene electrode and ionic liquid pinned on a bottom graphene grid electrode is described in Figure 1b. Under a low-pressure regime (less than a few kPa, Regime I), the ionic liquid droplet pinned on the graphene grid does not touch the top graphene electrode. Accordingly, the capacitance increases linearly with the applied pressure (**Figure 2**a). Note that a decrease in the dielectric displacement leads to an increase in the dielectric capacitance. The slope of the capacitance–pressure plot depends on the dielectric constant of the dielectric medium (in this case, air). Because the ionic liquid droplet is not in contact with the top graphene electrode, a change in the capacitance under pressure
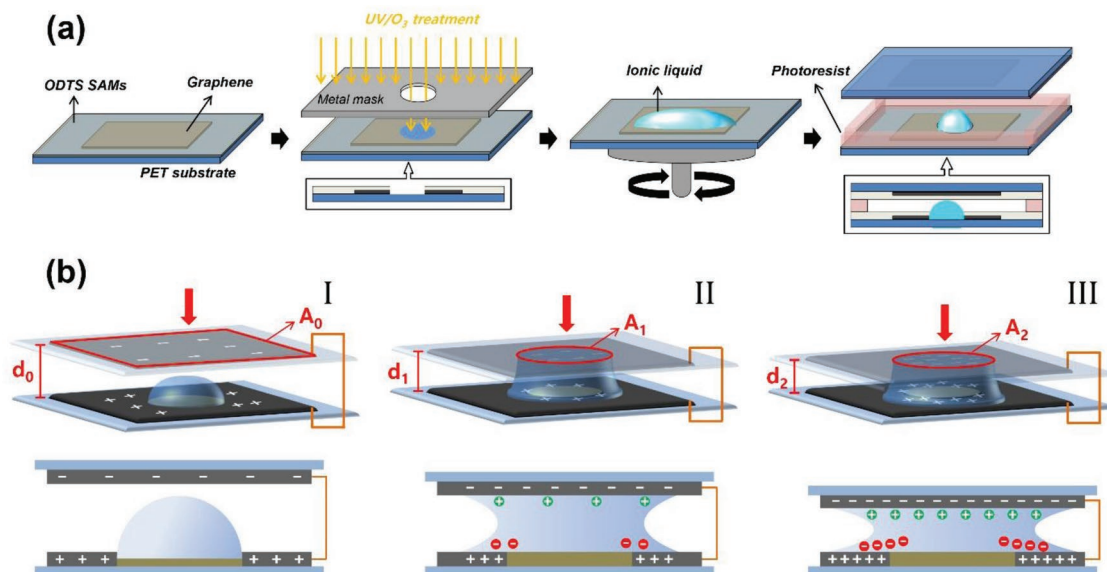

Figure 1. Preparation of the i-GTS and operating principle. a) Schematic illustration of the fabrication steps of the i-GTS with graphene and ionic liquid. b) Scheme showing the change in the device geometry (*A*: contact area, *d*: distance between electrodes) and accumulation of charge carriers in the capacitive-type i-GTS under applied pressure (I: air capacitance, II, III: EDL capacitance).
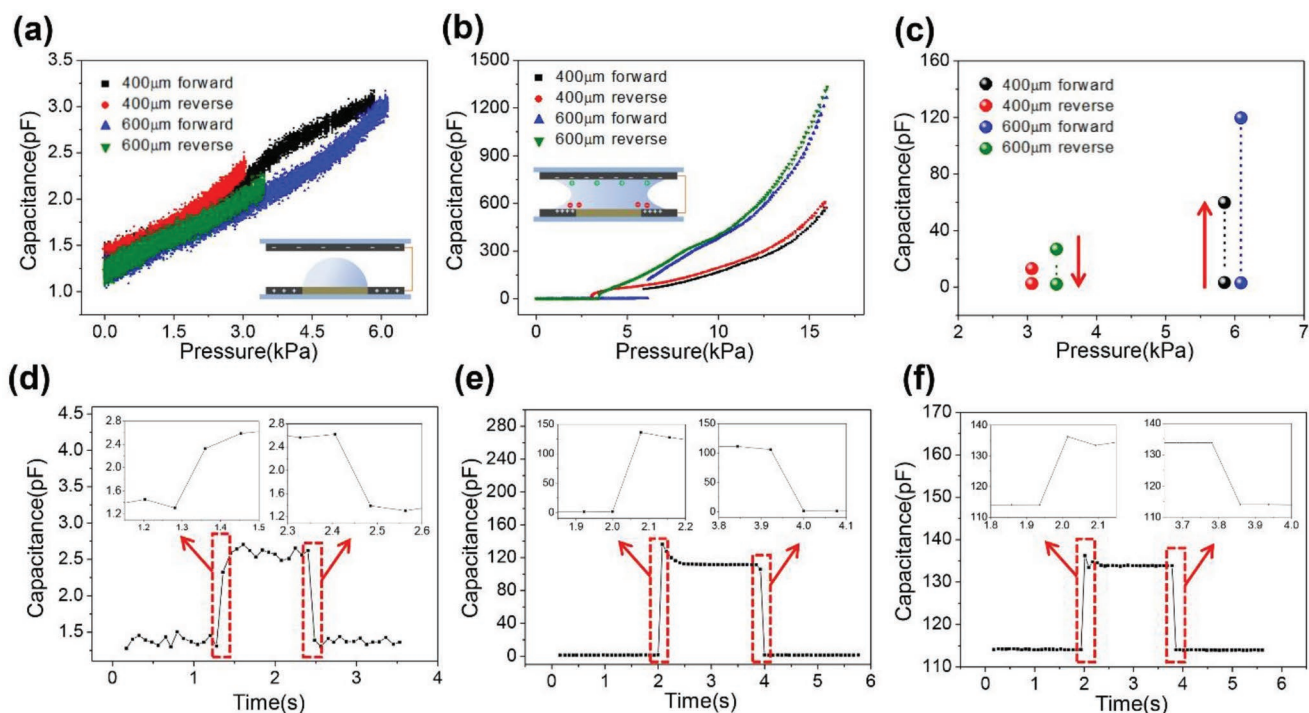
Figure 2. Pressure-sensing properties of the i-GTS. a,b) Pressure–capacitance curves in low-pressure regime and over the entire pressure regime. The changes in capacitance were recorded by applying (forward) and releasing (reverse) pressures on two different ionic liquid droplets (400 and 600 µm in diameter). c) Changes in capacitance at the contact point between the top electrode and ionic liquid. d–f) Response and relaxation curves of the fabricated i-GTS with 400 µm diameter droplet under the pressures of 4 kPa d) and 8 kPa e), and stepwise pressures of 8 and 10 kPa.

is affected by a change in the distance between the electrodes, and the droplet size has no effect. The spreading behavior of the ionic liquid contributes to a substantial increase in the capacitance when the ionic liquid droplet touches the top graphene electrode under prolonged pressure (≈6 kPa) (Figure 2b).

The huge increase in the capacitance of the i-GTS originates from the EDL induced in the ionic liquid droplet at the contact area of the graphene electrodes (Figure 1b, Regime II). The transitional states can be visualized by plotting the capacitance change at the pressure of the contact point. It can be noted that the transition pressure range of our i-GTS is in the gentle pressure regime (5–7 kPa), as shown in Figure 2b. To enhance the sensitivity, we can reduce the transition pressure by decreasing the distance between the electrodes and the elastic modulus of the substrate ((Equation (S1)) of the Supporting Information). In addition, larger diameter of droplet further increases the sensitivity (Equations (S2) and (S3) of the Supporting Information). We used diameter of the droplet because it can intuitively show the size of the droplet in comparison to electrode size. However, the diameter of the droplet can be converted to the droplet volume using Equation (S5) of the Supporting Information. Applying pressure (forward) causes a capacitance change from 3 pF (before contact) to 60 pF (after contact, ionic liquid droplet with 400 µm diameter) and 120 pF (after contact, liquid droplet with 600 µm diameter). This is because the volumetric effect of the ionic liquid droplet is related directly to the number of ions accumulated within the ionic liquid bridge at the contact area of the graphene electrodes in the i-GTS. Furthermore, interestingly, both the pressure and capacitance are lower at the

transition point in the reverse sweep, compared to that at the corresponding point in the forward sweep. This may be because the surface tension in the ionic liquid droplet delays the detachment of the ionic liquid droplet from the graphene electrode, decreasing both the transitional pressure and capacitance (compare Figure 2c left (reverse sweep) with Figure 2c right (forward sweep)). It should also be noted that the obtained transitional pressures can be decreased by using top and bottom plates with lower elastic moduli and by decreasing the gap between the ionic liquid and the top electrode.

Figure 2d–f shows the time-dependent response and relaxation curves of the fabricated i-GTS (with ionic liquid droplet of diameter 400 µm) under pressures of 4 kPa (Regime I) and 8 kPa (Regime I → II), and stepwise pressures of 8 and 10 kPa (Regime II → III). The response and relaxation curves of the i-GTS with ionic liquid droplets of diameter 600 µm are shown in Figure S4 of the Supporting Information. The defined pressure is applied during the time interval between 2 and 4 s. In Regime I, the change in dielectric displacement leads to instantaneous response and relaxation behaviors (Figure 2d). The full recovery of the relaxation behavior is mainly because of the cell design comprising graphene/PET at the top and bottom plates and polymer spacers at the edges of the cells, which retains sufficient restoring force. When 8 kPa is applied to the sensor, an abrupt increase in the capacitance, from 1 to 140 pF, is detected for 78 ms (Regime I → II, Figure 2e). This value is a resolution limit of our pressure sensor setup. We surmise that the transient response time will be shorter than 78 ms when using a sensitive instrument. The sensitivity of the i-GTS was calculated
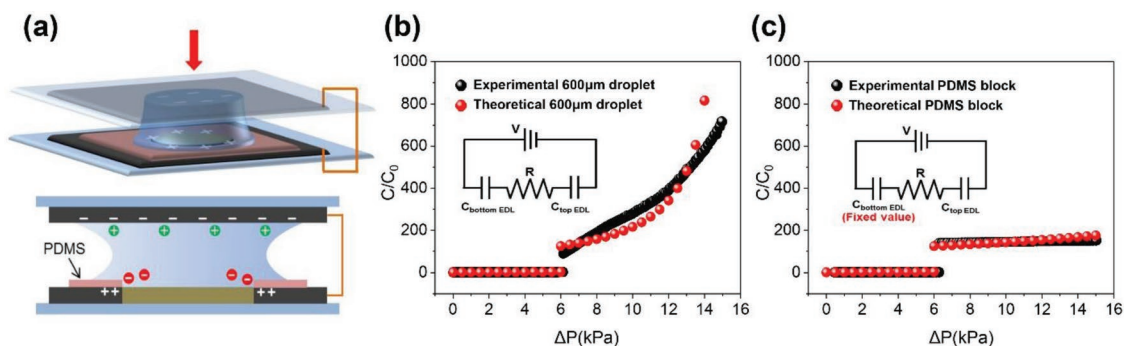
Figure 3. Comparison of experimental and theoretical sensing characteristics of the i-GTS in the EDL regime. a) Schematic of the i-GTS with bottom graphene grid blocked by PDMS. Experimental and theoretical plots of pressure-sensing properties in Figure 2b) (with 600 µm diameter) b) and the i-GTS with PDMS block c). Insets show the equivalent circuit diagrams of the i-GTS operated in the EDL regime.

to be 17.4 kPa^{-1}. This extremely high sensitivity is a result of a change in the capacitance mode (from air to EDL capacitance). The small decrease in the capacitance (from 140 to 120 pF) during a few hundreds of milliseconds after the initial loading is because of the restorative action of the ionic liquid bridge at the pinned graphene grid in the i-GTS, which contributes to a decrease in the ionic liquid–graphene grid contact area. Importantly, the i-GTS also exhibits a relaxation time of 78 ms under unloading, which is also the limit of our experimental setup. It has been reported that the viscoelastic behavior of the elastomer in the capacitive-type pressure sensor significantly increases the relaxation time under unloading.[6,9,15] The short relaxation time in our sensor originates directly from the use of an ionic liquid with viscosity lower than that of a sticky elastomer, such as poly(dimethylsiloxane) (PDMS) or ecoflex.[28,29] When a larger ionic liquid droplet with 600 µm diameter is used, a capacitance change from 1 to 250 pF is observed under a pressure of 8 kPa (Figure S4 in the Supporting Information). In this case, the sensitivity is calculated to be 31.1 kPa^{-1}, which is one of the highest values reported in the medium-pressure range (> a few kPa) so far (see Table S1 in the Supporting Information).[9,28–32] Although higher sensitivities have been reported in the previous reports, these values are typically obtained in extremely low pressure regimes (below 1 kPa).[33,34] For instance, the use of pyramidal ionic gels exhibited extremely high sensitivity of 41 kPa^{-1} at the low pressure below 0.4 kPa.[35] On the other hand, the sensitivity in the i-GTS can be improved by decreasing the gap between the ionic liquid droplet and graphene top electrode. The fabricated sensors exhibit acute response and relaxation times of 78 ms in all measurement ranges including the low-pressure regime (I), transition regime (I → II), and stepwise pressure application regime (II → III, Figure 2f).

The gradual increase in the capacitance after the contact between the ionic liquid and top graphene electrode can be related to the increase in the contact area between the ionic liquid and graphene electrodes (Figure 2b). Note that the capacitance is directly proportional to the contact area in the EDL system.[14,23] In our i-GTS setup, the top and bottom EDLs are combined linearly, as shown in Figure 2b inset; hence, the total capacitance can be calculated using the following Equation (1)[23]

$$1/C_{\text{total}} = 1/C_{\text{bottom EDL}} + 1/C_{\text{top EDL}} \qquad (1)$$

The contact area of the bottom EDL, where the ionic liquid is pinned on the graphene grid, is far smaller than the contact area of the top EDL. Thus, the capacitance in the bottom EDL is smaller than the capacitance in the top EDL. Accordingly, it is reasonable to speculate that an increase of the bottom EDL capacitance has a greater impact on the total capacitance change, than an increase in the top EDL. The ionic liquid bridge pinned on the graphene grid expands under applied pressure, leading to a gradual increase in the capacitance. To validate the mechanism of capacitance change in our EDL system (Regime II → III), the bottom graphene electrode (namely, the graphene grid) was blocked with PDMS (**Figure 3**a). Figure 3c shows the pressure-sensing properties of the PDMS-blocked i-GTS with ionic liquid droplet of diameter 600 µm. The pressure-sensing properties of the pristine i-GTS sensors without a PDMS block are also shown for comparison (Figure 3b). The i-GTS with PDMS block exhibits a similar jump in the capacitance at ≈6 kPa, which can be explained by the change in the capacitance mode (from air to EDL). However, the capacitance does not increase with prolonged pressure (>6 kPa). Although the ionic liquid expands under pressure and the top contact area increases, the contact area between the ionic liquid and bottom graphene grid electrode does not change because of the PDMS block. This is in stark difference with the cases of the pristine pressure sensors, which exhibit a gradual increase in the capacitance under prolonged pressure (>6 kPa). The control experiment clearly shows the operating mechanism of our tactile sensor in the EDL regime: contact line expansion with a corresponding increase in the contact area between the ionic liquid and graphene grid electrode. We also investigated the theoretical capacitance value of our i-GTS, based on plate theory about a rectangular plate[36] with simply supported ends (see Figure S5 and text in the Supporting Information). The pressure-induced deflection of top layer including graphene electrode and PET substrate causes the contact area change between the ionic liquid droplet and electrodes, thereby affecting the total EDL capacitance of the i-GTS. The small differences in the comparisons with the experimental capacitance values validate the proposed sensing mechanism in the EDL regime (Figure 3b,c).

Cyclic tests (300 cycles) with different sizes of ionic liquid droplets show that our sensors exhibit excellent stability in
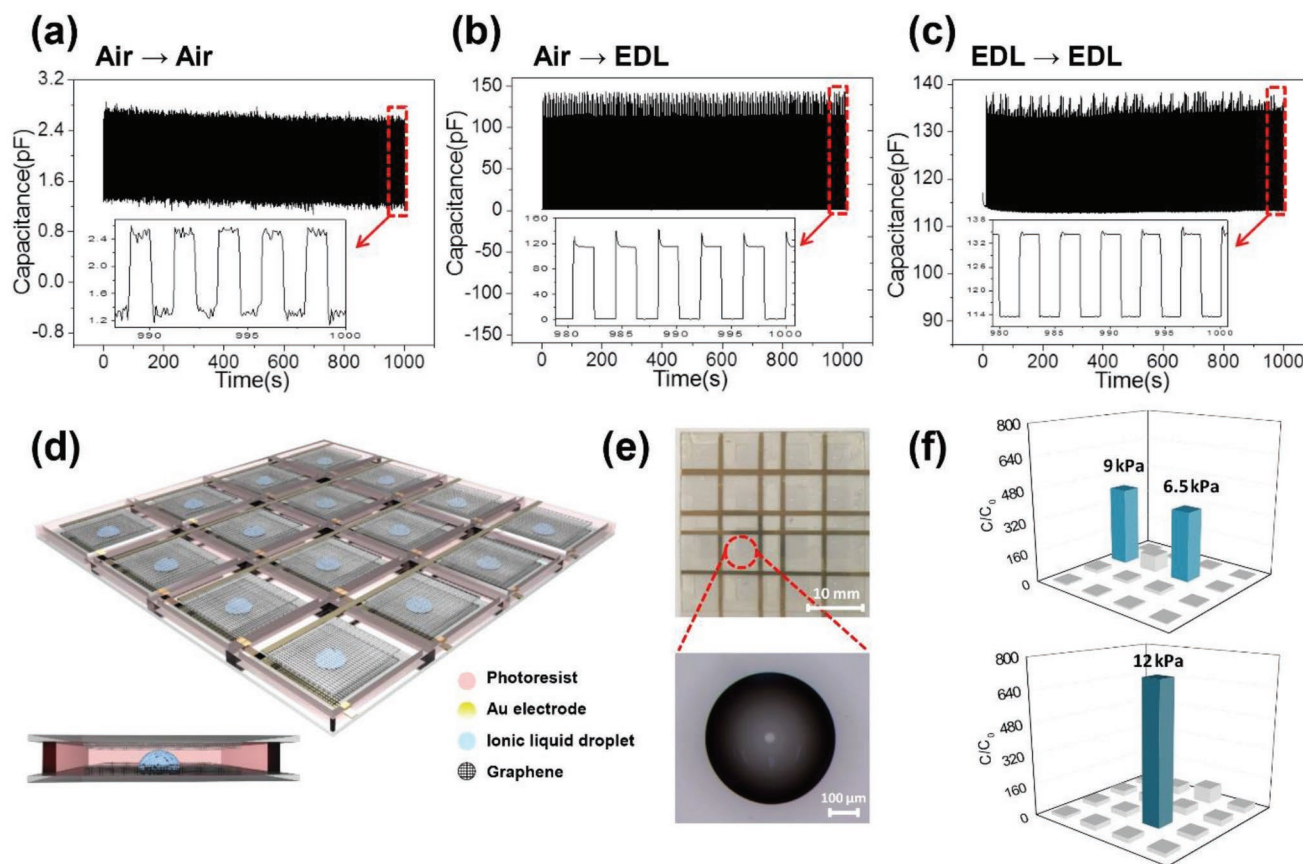
Figure 4. Cyclic and array tests using the i-GTS. a–c) Stability test (300 cycles) of the fabricated i-GTS with 400 μm diameter droplet under periodic pressures of 0 and 4 kPa a), 0 and 8 kPa b), and 8 and 10 kPa c). d) Photograph illustrates the components of the 4 × 4 pixel sensor array. e) Photograph of 4 × 4 pixel-type sensor array (scale bar, 10 mm) and the ionic liquid droplet in the unit pixel (scale bar, 100 μm). f) Pressure mapping of the i-GTS array on applying 6.5, 9 (multitouch response), and 12 kPa (single touch response) pressure at the given position.

all measurement regimes, including I, I → II, and II → III regimes (**Figure** 4a–c; and Figure S6 in the Supporting Information). All the elements in the i-GTS sensors are environmentally stable and mechanically flexible. The ionic liquid used in this experiment exhibits extremely low vapor pressure,[20,37] indicating long-term stability under ambient conditions, which is appropriate for an active element in a tactile sensor. In addition, no remaining ionic liquid satellites on the top electrode surface are detected after dynamic cyclic tests. This may be because of the combined effect of an ionic liquid with low viscosity and the hydrophobic surface of the top electrode treated with ODTS. When different types of ionic liquids with higher viscosities were tested, it was observed that the viscous properties prohibited reproducibility of the i-GTS performances. We then fabricated a 4 × 4 pixel-type i-GTS array, as shown in Figure 4d. The array has 5 × 5 mm² sensing area per pixel with center-to-center distance of 7 mm. The detailed dimensions of the ionic liquid droplet in the unit pixel are characterized by optical microscope in top view, showing 600 μm diameter and 140 μm height, provided the droplet volume of 0.1 μL, as shown in Figure 4e. The height and volume of the ionic liquid droplets were calculated by a general relationship between the geometry parameters and the contact angle of an intersected sphere (see Figure S7 and text in the Supporting

Information). The fabricated i-GTS array exhibited excellent pressure-mapping characteristics without any interference from neighboring cells (Figure 4f). This outstanding performance is mainly due to the operating mechanisms that are applicable differently to different cells. The neighboring cells are still in the air-capacitance regime (I), while the pressure-applied cell operates in the EDL capacitance regime (II). The signal-to-noise ratio (SNR) is extremely high, when compared to that of the traditional elastomer-based capacitive-type sensors. This means that our i-GTS will be beneficial for the design of transparent and flexible touch-panel displays where high sensitivity, fast response time, and high SNR are necessary over a wide working pressure range. In addition, we have evaluated the mechanical flexibility and reliability of the i-GTS array as a function of the radius of curvature of 26.3, 18.6, 15.1, and 13.1 mm (see Figure S9 in the Supporting Information). The capacitance under various pressures (5, 10, and 15 kPa) remains unchanged after 10 000 bending cycles at 1.3% effective strain. Recently, elastomer-based microfluidic system was devised for the development of liquid-state stretchable sensors.[25] This type of sensor is beneficial for the enabling stretchable tactile sensors.[38] Further work relating to cell design is necessary for the development of stretchable i-GTS.

**ADVANCED
SCIENCE NEWS**
www.advancedsciencenews.com

**ADVANCED
FUNCTIONAL
MATERIALS**
www.afm-journal.de

3. Conclusion

In summary, transparent and flexible i-GTS were fabricated using an ionic liquid droplet pinned on a graphene grid. When mechanical stress was applied to the top floating graphene electrode, the capacitive-type i-GTS were operated in three different modes (i.e., air → air, air → EDL, EDL → EDL). When pressure of a few kPa was applied to the i-GTS, the top electrode did not touch the ionic liquid droplet and the dielectric displacement of air led to an increase in the capacitance. The top electrode touched the ionic liquid under pressures exceeding 6 kPa and the spreading of the ionic liquid resulted in a capacitance jump, which was caused by EDL formation in the contact area of the ionic liquid. Under prolonged pressure, the capacitance of the i-GTS increased gradually, mainly because of the contact line expansion of the ionic liquid bridge pinned on the graphene grid. The response and relaxation analyses at these three regimes indicated that the i-GTS exhibited a prompted response and relaxation time of 78 ms, which was the minimum value in our experimental setup. The sensitivity was increased up to 31.1 kPa^{-1} by utilizing the transition of the capacitance mode from air to EDL, when the applied pressure was within the gentle touch region. Cyclic tests proved the long-term stability while array tests exhibited extremely high SNR. The i-GTS proposed in this work can enhance the sensor properties (i.e., response time, sensitivity, and SNR) greatly by using the transition from air to EDL, which is driven by the spreading of the ionic liquid. Further optimization can lead to investigation of interesting phenomena, such as 3D touch when using liquid-based materials.

4. Experimental Section

Materials and Sensor Fabrication: High-quality monolayer graphene was grown by CVD.[39,40] The graphene on Cu foil was transferred onto a (from SKC Co.) substrate (100 μm thickness) through a poly(methyl methacrylate) (PMMA from Aldrich Co.)-supported transfer method.[41] After successful transfer of the graphene to the PET substrate, the PMMA on the graphene surface was removed by soaking PMMA/graphene/PET into acetone. The graphene surface was treated with octadecyltrichlorosilane (ODTS from Gelest Co.) to increase its hydrophobicity. The ODTS/graphene at the center region was etched selectively by treating the UV/Ozone (AHTECH Co. AH1700) with a metal shadow mask. 1-Ethyl-3-methylimidazolium tetrafluoroborate ([EMIM]$^+$[BF$_4$]$^-$ from Aldrich Co.) was patterned on the ODTS/graphene grid by spin-casting. Photolithography with SU-8 photoresist (MicroChem Co.) and 365 nm UV light was used for fabricating the spacer (300 μm thickness) at the edges of the patterned [EMIM]$^+$[BF$_4$]$^-$/ODTS/graphene/PET. The top floating plate of the sensor was fabricated using ODTS/graphene/PET. Finally, the top and bottom plates were attached mechanically and the wirings of the top and bottom plates were attached using thin Ag wires. A 4 × 4 pixel-type sensor array was fabricated by integrating 16 cells.

Characterization: The structural characteristics of graphene upon ODTS deposition and UV/Ozone exposure were analyzed with a Raman spectroscope (Witec alpha 300R) using a 532 nm laser. A SiO$_2$/Si substrate was used instead of a PET substrate for obtaining enhanced Raman signals. The surface energies of graphene and ODTS/graphene were calculated by measuring the contact angles of the probe liquids with a contact-angle meter (SEO Phoenix 300 Touch). The change in the droplet shape under pressure was visualized using an optical microscope and CCD camera. A gauge force meter (M5-05, Mark-10) and LCR meter (4980A, Keysight Technologies) were connected to a semiconductor parameter analyzer (4200-SCS Source Measure Unit, Keithley) to record the time-dependent capacitance–pressure curves. Force was applied to the sensors with an axis motion controller, while a gauge force meter and LCR meter simultaneously detected the force and capacitance, respectively. The stability of the sensors was tested by repeating 300 cycles over the defined pressure ranges. Transmittance spectra of the Single and double layers PET/Graphene were recorded on a spectrophotometer (Cary 60 UV–Vis, Agilent).

Bending Test: The mechanical reliability of the capacitive-type pressure sensors was measured using 2-axis motion controllers (STM-2-USB, ST1), which was connected bending machine system (ST-BJS-0810-SSU, ST1). Test speed was fixed at 0.3 mm s^{-1}.

Supporting Information

Supporting Information is available from the Wiley Online Library or from the author.

Conflict of Interest

The authors declare no conflict of interest.

[1] D. J. Lipomi, M. Vosgueritchian, B. C. K. Tee, S. L. Hellstrom, J. A. Lee, C. H. Fox, Z. Bao, *Nat. Nanotechnol.* **2011**, *6*, 788.

[2] J. Park, Y. Lee, J. Hong, Y. Lee, M. Ha, Y. Jung, H. Lim, S. Y. Kim, H. Ko, *ACS Nano* **2014**, *8*, 12020.

[3] S. Chen, K. Jiang, Z. Lou, D. Chen, G. Shen, *Adv. Mater. Technol.* **2018**, *3*, 1700248.

[4] L. Nela, J. Tang, Q. Cao, G. Tulevski, S.-J. Han, *Nano Lett.* **2018**, *18*, 2054.

[5] C.-B. Huang, S. Witomska, A. Aliprandi, M.-A. Stoeckel, M. Bonini, A. Ciesielski, P. Samorì, *Adv. Mater.* **2019**, *31*, 1804600.

[6] M. L. Hammock, A. Chortos, B. C. K. Tee, J. B. H. Tok, Z. Bao, *Adv. Mater.* **2013**, *25*, 5997.

[7] X. Wang, L. Dong, H. Zhang, R. Yu, C. Pan, Z. L. Wang, *Adv. Sci.* **2015**, *2*, 1500169.

**ADVANCED
SCIENCE NEWS**

www.advancedsciencenews.com

**ADVANCED
FUNCTIONAL
MATERIALS**

www.afm-journal.de

[8] Y. Lee, J. Park, A. Choe, S. Cho, J. Kim, H. Ko, *Adv. Funct. Mater.* **2019**, https://doi.org/10.1002/adfm.201904523.

[9] S. C. B. Mannsfeld, B. C. K. Tee, R. M. Stoltenberg, C. V. H. H. Chen, S. Barman, B. V. O. Muir, A. N. Sokolov, C. Reese, Z. Bao, *Nat. Mater.* **2010**, *9*, 859.

[10] S. Y. Kim, S. Park, H. W. Park, D. H. Park, Y. Jeong, D. H. Kim, *Adv. Mater.* **2015**, *27*, 4178.

[11] J. Lee, H. Kwon, J. Seo, S. Shin, J. H. Koo, C. Pang, S. Son, J. H. Kim, Y. H. Jang, D. E. Kim, T. Lee, *Adv. Mater.* **2015**, *27*, 2433.

[12] H. Jang, H. Yoon, Y. Ko, J. Choi, S.-S. Lee, I. Jeon, J.-H. Kim, H. Kim, *Nanoscale* **2016**, *8*, 5667.

[13] Y. Zang, F. Zhang, C.-a. Di, D. Zhu, *Mater. Horiz.* **2015**, *2*, 140.

[14] J. Heikenfeld, A. Jajack, J. Rogers, P. Gutruf, L. Tian, T. Pan, R. Li, M. Khine, J. Kim, J. Wang, J. Kim, *Lab Chip* **2018**, *18*, 217.

[15] Z. Ma, S. Li, H. Wang, W. Cheng, Y. Li, L. Pan, Y. Shi, *J. Mater. Chem. B* **2019**, *7*, 173.

[16] K. F. Lei, K.-F. Lee, M.-Y. Lee, *Microelectron. Eng.* **2012**, *99*, 1.

[17] T. Li, H. Luo, L. Qin, X. Wang, Z. Xiong, H. Ding, Y. Gu, Z. Liu, T. Zhang, *Small* **2016**, *12*, 5042.

[18] X. Shuai, P. Zhu, W. Zeng, Y. Hu, X. Liang, Y. Zhang, R. Sun, C.-p. Wong, *ACS Appl. Mater. Interfaces* **2017**, *9*, 26314.

[19] B. Nie, S. Xing, J. D. Brandt, T. Pan, *Lab Chip* **2012**, *12*, 1110.

[20] B. Nie, R. Li, J. D. Brandt, T. Pan, *Lab Chip* **2014**, *14*, 1107.

[21] B. Nie, R. Li, J. D. Brandt, T. Pan, *Lab Chip* **2014**, *14*, 4344.

[22] B. Nie, R. Li, J. Cao, J. D. Brandt, T. Pan, *Adv. Mater.* **2015**, *27*, 6055.

[23] M. L. Jin, S. Park, Y. Lee, J. H. Lee, J. Chung, J. S. Kim, J.-S. Kim, S. Y. Kim, E. Jee, D. W. Kim, J. W. Chung, S. G. Lee, D. Choi, H.-T. Jung, D. H. Kim, *Adv. Mater.* **2017**, *29*, 1605973.

[24] Y. Gao, H. Ota, E. W. Schaler, K. Chen, A. Zhao, W. Gao, H. M. Fahad, Y. Leng, A. Zheng, F. Xiong, C. Zhang, L.-C. Tai, P. Zhao, R. S. Fearing, A. Javey, *Adv. Mater.* **2017**, *29*, 1701985.

[25] H. Ota, K. Chen, Y. Lin, D. Kiriya, H. Shiraki, Z. Yu, T.-J. Ha, A. Javey, *Nat. Commun.* **2014**, *5*, 5032.

[26] B. Lee, Y. Chen, F. Duerr, D. Mastrogiovanni, E. Garfunkel, E. Y. Andrei, V. Podzorov, *Nano Lett.* **2010**, *10*, 2427.

[27] B. Kang, S. K. Lee, J. Jung, M. Joe, S. B. Lee, J. Kim, C. Lee, K. Cho, *Adv. Mater.* **2018**, *30*, 1706480.

[28] S. Baek, H. Jang, S. Y. Kim, H. Jeong, S. Han, Y. Jang, D. H. Kim, H. S. Lee, *RSC Adv.* **2017**, *7*, 39420.

[29] K. Lee, J. Lee, G. Kim, Y. Kim, S. Kang, S. Cho, S. Kim, J.-K. Kim, W. Lee, D.-E. Kim, S. Kang, D. Kim, T. Lee, W. Shim, *Small* **2017**, *13*, 1700368.

[30] Y.-S. Chen, G.-W. Hsieh, S.-P. Chen, P.-Y. Tseng, C.-W. Wang, *ACS Appl. Mater. Interfaces* **2015**, *7*, 45.

[31] B.-Y. Lee, J. Kim, H. Kim, C. Kim, S.-D. Lee, *Sens. Actuators, A* **2016**, *240*, 103.

[32] A. Chhetry, H. Yoon, J. Y. Park, *J. Mater. Chem. C* **2017**, *5*, 10068.

[33] A. Chhetry, J. Kim, H. Yoon, J. Y. Park, *ACS Appl. Mater. Interfaces* **2019**, *11*, 3438.

[34] J. C. Yang, J.-O. Kim, J. Oh, S. Y. Kwon, J. Y. Sim, D. W. Kim, H. B. Choi, S. Park, *ACS Appl. Mater. Interfaces* **2019**, *11*, 19472.

[35] S. H. Cho, S. W. Lee, S. Yu, H. Kim, S. Chang, D. Kang, I. Hwang, H. S. Kang, B. Jeong, E. H. Kim, S. M. Cho, K. L. Kim, H. Lee, W. Shim, C. Park, *ACS Appl. Mater. Interfaces* **2017**, *9*, 10128.

[36] Young, W. Clarence, R. G. Budynas, A. M. Sadegh, *Roark's Formulas for Stress and Strain*, Vol. *4*, McGraw-Hill, New York **2002**.

[37] R. Li, B. Nie, P. Digiglio, T. Pan, *Adv. Funct. Mater.* **2014**, *24*, 6195.

[38] Y. -L. Park, B. -R. Chen, R. J. Wood, *IEEE Sens. J.* **2012**, *12*, 2711.

[39] X. Li, W. Cai, J. An, S. Kim, J. Nah, D. Yang, R. Piner, A. Velamakanni, I. Jung, E. Tutuc, S. K. Banerjee, L. Colombo, R. S. Ruoff, *Science* **2009**, *324*, 1312.

[40] H. C. Lee, S. B. Jo, E. Lee, M. S. Yoo, H. H. Kim, S. K. Lee, W. H. Lee, K. Cho, *Adv. Mater.* **2016**, *28*, 2010.

[41] W. H. Lee, J. Park, S. H. Sim, S. Lim, K. S. Kim, B. H. Hong, K. Cho, *J. Am. Chem. Soc.* **2011**, *133*, 4447.